Coastal protection by a small scale river plume against oil spills in the Northern Gulf of Mexico

Kuitenbrouwer, Daan; Reniers, Ad; MacMahan, Jamie; Roth, Mathias K.

DOI
10.1016/j.csr.2018.05.002

Publication date
2018

Document Version
Final published version

Published in
Continental Shelf Research

Citation (APA)
Kuitenbrouwer, D., Reniers, A., MacMahan, J., & Roth, M. K. (2018). Coastal protection by a small scale river plume against oil spills in the Northern Gulf of Mexico. *Continental Shelf Research*, *163*, 1-11. https://doi.org/10.1016/j.csr.2018.05.002

Continental Shelf Research 163 (2018) 1–11

Contents lists available at ScienceDirect

Continental Shelf Research

journal homepage: www.elsevier.com/locate/csr

Coastal protection by a small scale river plume against oil spills in the Northern Gulf of Mexico

Daan Kuitenbrouwer[a,*], Ad Reniers[a], Jamie MacMahan[b], Mathias K. Roth[b]

[a] Delft University of Technology, Stevinweg 1, 2628 CN Delft, The Netherlands
[b] Oceanography Department, Naval Postgraduate School, 1 University Circle, Monterey, CA 93943, United States

ARTICLE INFO

Keywords:
River plume
Surface material transport
Inner shelf
Coastal barriers
Oil spill

ABSTRACT

The Deepwater Horizon oil spill damaged some beaches along the Northern Gulf of Mexico (NGoMex) coast more than others, possibly related to the presence of natural protection mechanisms. In order to optimize future mitigation efforts to protect the coast, these mechanisms should be understood. The NGoMex coast is characterized by relatively long stretches of sandy beach interrupted by tidal inlets creating ebb-tidal river plumes featuring frontal zones that may act as transport barriers. This research investigates to what extent these plumes are capable of protecting the adjacent coast. This is done by means of a combination of a 3D Eulerian flow model and a Lagrangian particle model to track oil pathways and visualize Lagrangian Coherent Structures located at the plume front. The models are verified with measurements from a field experiment adjacent to Destin Inlet, Florida. The effects of wind, tidal range and river discharge on the oil fate are discussed. It was found that wind is the dominant parameter. Offshore wind prevents oil from beaching. During onshore winds, oil is pushed to shore, but near the inlet the plume is effective in reducing the amount of oil washing ashore during the ebbing tide. In general, the plume redistributes the oil but is not capable of preventing oil from beaching. For strong winds, the influence of the plume is reduced.

1. Introduction

The Deepwater Horizon oil spill caused severe damage to many coastal ecosystems in the Northern Gulf of Mexico (NGoMex) (Upton, 2011). Despite much effort being made in cleaning up the oil before it washed ashore, it was impossible to protect all coastal systems because of the sheer quantity of spilled oil in comparison to the means of cleaning (Graham et al., 2011; Smithsonian, 2016). Moreover, the spreading and mixing of surface material is not well modeled at the submesoscale (1–10 km) by circulation models (Poje et al., 2014; Gildor et al., 2009) resulting in uncertainties on where and when oil will wash ashore (Roth et al., 2017).

In order to reduce the damage of oil spills, first responders should be pointed to those patches of oil that are most harmful to coastal ecosystems and have greatest socio-economic impact, that is, the patches of oil that wash ashore (Smith et al., 2010; Morris et al., 2013; Huguenard et al., 2016). Understanding where these patches of oil come from requires a thorough understanding of the circulation on the inner shelf, which is the zone where the turbulent surface and bottom boundary layer overlap (Lentz and Fewings, 2012) and reaches from the surfzone to approximately 30 m water depth (Kennish, 2000), which is >20 km offshore for the biggest portion of the coast in the NGoMex. The most important forcing mechanisms on the inner shelf are wave-, wind- and tidal forcing in general, however the influence of rivers forming brackish buoyant plumes can be important as well (Lentz and Fewings, 2012; Horner-Devine et al., 2015; Xia et al., 2011). In a study on the effects of the Mississippi river plume, Kourafalou and Androulidakis (2013) found that onshore transport was restrained due to circulations related such a plume. Roth et al. (2017) has shown that the wind driven plume of the Choctawhatchee bay is an effective barrier for surface drifters and is therefore expected to prevent offshore surface pollution from washing ashore. His findings were derived from data from the Surfzone and Coastal Oil Pathways Experiment (SCOPE), a two week field experiment near Destin, Florida in December 2013. During SCOPE, an ADCP and a CTD array were deployed at location A in Fig. 1 to measure flow velocity and salinity. The array was positioned perpendicular to the coast, consisted of six stations and ranged from the beach to 500 m offshore where the water depth is 10 m. The locations and bottom levels of the stations in the array are also shown in Fig. 1. Besides that, surface drifters were deployed and their paths were tracked. As SCOPE lasted two weeks, there was only a limited set of forcing conditions.

* Corresponding author.
E-mail address: daankuitenbrouwer@gmail.com (D. Kuitenbrouwer).

https://doi.org/10.1016/j.csr.2018.05.002
Received 11 June 2017; Received in revised form 30 April 2018; Accepted 9 May 2018
Available online 12 May 2018

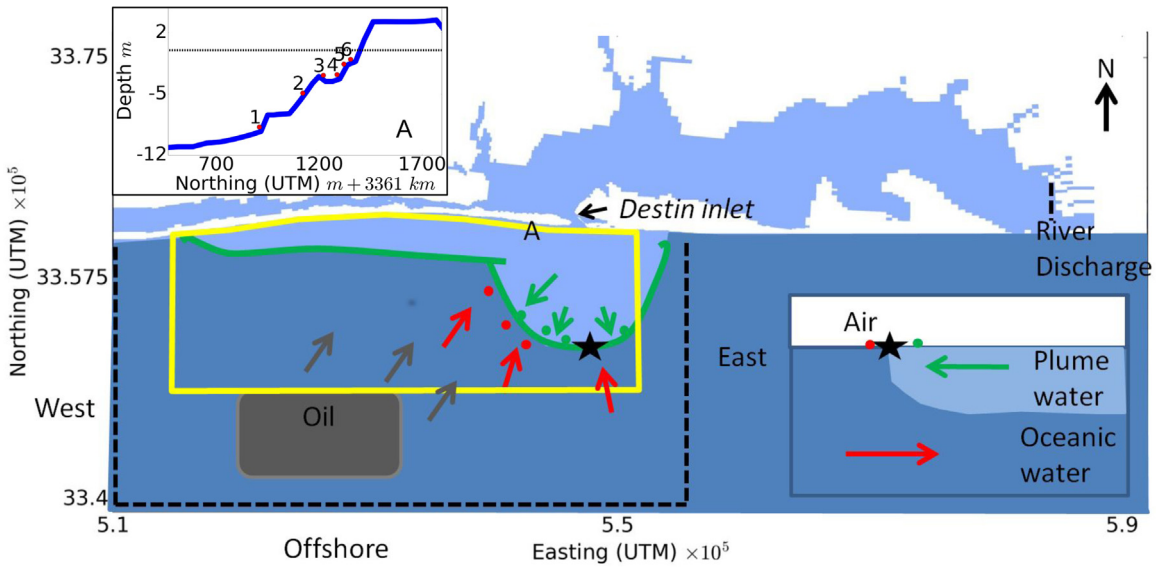

Fig. 1. Overview of the research domain and the buoyant plume. The light blue water denotes brackish water from the bay, whereas the darker blue denotes oceanic saline water. Green and red arrows and dots refer to the movement of particles within the plume and oceanic waters respectively. The green line highlights the edge of the plume waters, where surface flotsam is expected to gather. The boundaries of the Eulerian flow model are shown as the black dashed line and are named West, Offshore, East and River Discharge. The yellow shape shows the initial position of Lagrangian tracers and is therefore the area within which LCS can be calculated. The inset in the left upper corner shows the sea bed level of the measurement stations in the cross-shore measurement array during SCOPE at location A. Figure adjusted from Roth et al. (2017) and Huguenard et al. (2016).

This work makes use of the findings of SCOPE and goes one step further by creating a broader understanding on the plume related coastal protection against offshore oil for various wind forcings, tidal ranges and river discharges. An Eulerian flow model (Delft3D) is used to calculate pathways of Lagrangian tracers, allowing for the calculation of Lagrangian Coherent Structures (LCS). In a theoretical work, Shadden (2006) found that the flux through LCS is negligible when they are properly defined. In accordance with the findings of Roth et al. (2017), plume fronts may form barriers through which no transport occurs, hence they should show up as LCS. This method has been used to visualize the location and evolution of transport barriers in systems on the scale of rip currents $O(100\,m)$ (Reniers et al., 2010), driven by waves and with time scales on the order of 10 min. Also, the method has been used on the scale of a bay $O(1\,km)$ (Fiorentino et al., 2012), with the dominant forcing being a semidiurnal tide. Lastly, the method has been shown to be useful up to the oceanic mesoscales on the order of $O(100\,km)$ (Olascoaga et al., 2013) driven by various types of oceanic forcings on the order of weeks, showing that the method is useful over a wide range of forcing types and time scales. In this work, the LCS are used to visualize flow features rather than finding barriers through which no transport at all occurs.

Lagrangian tracers serve to understand where oil beaches and where it comes from. Consequently, the positions of the plumes together with data on where oil beaches is used to get a better idea on the actual coastal protection due to the plume for various forcing sets. This can then be used as a guide for first responders on how to use their resources most effectively in reducing damage to the coastal ecosystem.

In the following, the domain of research - the NGoMex and the Choctawhatchee bay - are discussed, followed by the protection mechanism of the plume. The numerical models are discussed to a greater extent and they are verified with data from SCOPE. Lastly it is discussed how the Choctawhatchee plume protects the coast and how first responders can make use of these findings.

2. The buoyant plume of the Choctawhatchee bay as a coastal protection mechanism

The Choctawhatchee river plume is a small-scale river plume (Huguenard et al., 2016). River plumes are driven by density gradients which are a result of fresh river water. The fate of such plumes is influenced by many factors such as tides, ambient currents, Coriolis, wind, river discharge, the bathymetry and the angle between the coastline and the inlet feeding into it (Horner-Devine et al., 2009; Bianchi et al., 2013).

Horner-Devine et al. (2015) describe the spatial evolution of a river plume in terms of four different dynamically defined zones. The first zone is the source zone in the estuary, where the dynamics are determined by estuarine processes. The second zone is the near-field where the flow is steered by inertia, both barotropic- and baroclinic pressure gradients and deceleration through turbulent stress with the ambient water. In this zone the flow is supercritical, that is, the Froude number is greater than one, $Fr = U/c_i > 1$, with U the flow velocity and c_i the internal wave speed. Therefore the near-field often features a sharp frontal boundary with strong surface convergence (Garvine, 1984; Garvine and Monk, 1974; O'Donnell et al., 1998). At the point where the Froude number drops below one, the near-field ends (Hetland, 2005) and the mid-field starts. In this field the dynamics are dominated by the Earth's rotation and wind steering and the inflow momentum is lost. In the mid-field, the plume often forms a shore parellel coastal current as a result of Coriolis (Garvine, 1987) or ambient alongshore currents (Fong and Geyer, 2002). The last zone is the far-field. In this field there is no remembrance of the inflow momentum and the plume is steered by the Earth's rotation, buoyancy and wind (Horner-Devine et al., 2015). Turbulent mixing of the plume with ambient water due to wind can be substantial in all zones. The strength of mixing at the plume front in the near field is often orders of magnitude greater than due to wind, however as the wind affects the entire plume and hence a large spatial area wind effects remain important (Horner-Devine et al., 2015).

The Choctawhatchee bay is located in the NGoMex, it is approximately 43 km long, on average 5 km wide and it is relatively shallow with an average depth of 4 m (Valle-Levinson et al., 2015; Schaeffer, 2010). The Destin inlet is the connection between the gulf and the bay and is ~ 450 m wide and 7 m deep. The Choctawhatchee river feeds into the bay on the Eastern end, as shown in Fig. 1. An analysis of volumetric river flux data from 2007 to 2016 from USGS station 02365500

upstream shows that the minimum, average and maximum river flux are respectively 32.3, 188.3 and 2183.2 m^3/s (USGS, 2016). Winds are predominantly light (<3 m/s) and from the Southwest during the summer (Velasco and Winant, 1996). During the winter winds are steered by extratropical cyclones (Roth, 2016). These extratropical cyclones - or cold air outbreaks (CAO) - bring cold air from the North and are accompanied with cold fronts (Marmorino, 1982; Velasco and Winant, 1996; Huh et al., 1984). The wave climate in the NGoMex is weak in general owing to the limited fetch. An analysis of wave data from wavebuoy 42012, 23 km off Orange Beach, AL shows that during the summer significant wave heights are mainly between 0.5 and 1 m with periods between 4 and 6 s coming from the Southern quarter of the windrose. During the winter there is more variation, but significant wave heights rarely exceed 2 m and periods mostly remain below 8 s (NOAA, 2017). During hurricanes, wind, wave heights and periods become much greater, these conditions are not considered in this research. Tides are diurnal (Seim et al., 1987) with a tidal range varying between 0.2 and 0.7 m and a mean of 0.5 m (Murphy et al., 2009).

Besides these external factors, the evolution of the plume is influenced by mixing with oceanic waters for which the mixing budget is discussed in Huguenard et al. (2016) and ambient background flows. The largest flow structures in the Gulf of Mexico are related to the loop current which sheds off large anticyclonic eddies (Hurlburt and Thompson, 1982). However, their influence on the coastal zones is limited due to the width of the shelf (Marmorino, 1982). The greatest influence of ambient background currents comes from flow reversals which are related to the Northerly winds from CAO's (Mitchum and Clarke, 1986; Hsueh and Golubev, 2002). Roth (2016) describes the full depth flow reversals - flow to the West under winds to the North before frontal passage reversing to flow to the East under winds to the South after frontal passage - as an ageostrophic response to wind driven setup / setdown and finds a variation of alongshore flow velocity of 0.3 m/s within 3 h.

Regarding the protection mechanisms, oil may be retained from washing ashore by the near-field front as it features convergence of surface flow. This leads to oil concentrating at these lines of convergence - the fronts, which was shown by making use of surface drifters by Roth et al. (2017). This process is described in the inset of Fig. 1. In the mid- and far field, where fronts are weaker and yield less surface convergence, oil may still be prevented from reaching the shore due to deflection by the coastal current which flows alongshore.

As mentioned earlier, the plume itself is influenced by the wind. Besides that, wind also directly influences the fate of oil. The interaction between oil, wind and waves is highly complex and depends on the type of oil (Reed et al., 1994). In the case of light winds, $\vec{u}_w < 6\ m/s$, oil drifts downwind with a velocity of approximately 3% of the wind speed and remains at the surface (Reed et al., 1999). For a wind speed of 3 $\mathbf{m/s}$, a contribution of the wind on the velocity of oil of 0.1 $\mathbf{m/s}$ is thus expected, which is on the order of the ambient currents. It can hence be noted that windage is a very important parameter when considering oil transport. One can thus anticipate that offshore winds push oil offshore and for strong enough winds prevent it from washing ashore. On the other hand, it becomes interesting to see to what extent the plume front and coastal current are capable of preventing oil from beaching under onshore winds. As these processes are very complex and the strength of the barrier at the plume fronts in terms of their capacity of preventing oil from crossing them varies with time and space, one needs to resort to numerical modeling to get a clear overview on the extent to which coasts are protected against offshore oil under given forcing.

3. Numerical methods

3.1. Eulerian flow model - Delft3D

Delft3D (D3D) is an open source modeling suite that can be used to investigate hydrodynamics for coastal environments (Lesser et al., 2004). D3D's FLOW module solves the non-linear unsteady shallow water equations taking Coriolis into account and a constituent transport equation. For this work turbulence was resolved with a k-ϵ model. The grid is a curvilinear orthogonal grid in the horizontal and consists of 151 by 260 cells spanning ~ 86 km in the zonal and 30 km in the meridional direction (see Fig. 1). The smallest cells are 60 m (zonal) by 30 m (meridional), whereas the largest cells are 2.5 km (zonal) by 600 m (meridional) far away from the inlet. The maximum difference in size between neighbouring grid cells is 20% in order to reduce numerical inaccuracies. In the vertical, the model consists of 14 sigma layers. The thickness of these layers is determined as an equivalent of the total depth. These equivalents are 2, 3, 4, 6, 8, 10, 12, 15, 12, 10, 8, 5, 3, 2% respectively. This setup was chosen to accurately model the thin top layer where the plume resides as well as the near bed flow structure. The model was forced with wind stress that is quadratically related to the wind speed and a wind speed dependent drag factor (Smith and Banke, 1975). The tide is imposed on the lateral East and West boundaries with a combination of Neumann and Riemann boundary conditions and a weakly reflective alongshore varying water level at the offshore boundary to account for ambient currents associated with CAOs (see appendix A). The river inflow is modeled as a freshwater discharge at the Eastern end of the bay. Bottom friction is taken into account through a Manning factor with $n = 0.028$. Baroclinic pressure gradients driving the plume are taken into account due to differences in salinity as the model is run in baroclinic mode. The initial setup of the model consisted of a constant salinity throughout the bay of 21 ppt inside the bay and 35 ppt outside the bay - the spin-up time was 2 weeks. For later simulations, the initial setup was taken as the setup after 2 weeks of spin up and an extra day of spin-up was used to allow the system to adjust to the new forcing. The same model was applied for a study on the frontal zone of the plume in Huguenard et al. (2016), which describes the model more in depth.

The skill of the model is verified with the cross-shore array measurements during the field experiment (SCOPE) in Figs. 2 and 3. The skill of the model is given in Table 1, and calculated as follows,

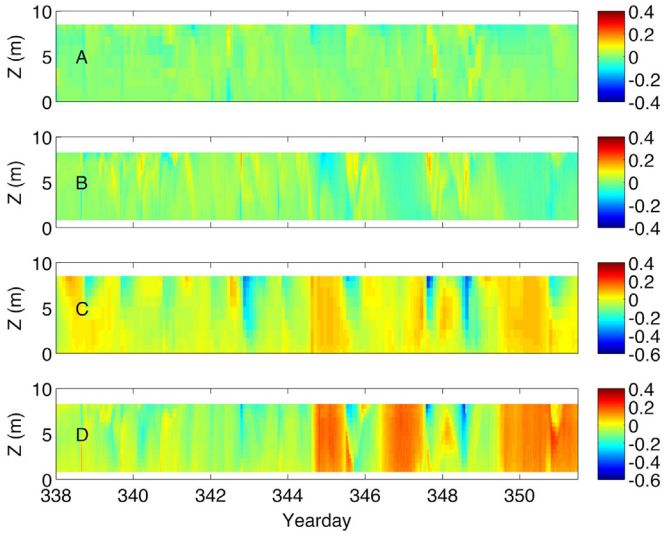

Fig. 2. Verification of the time and depth dependent flow (m/s) simulated by D3D with measurements during SCOPE at position A, station 1 in Fig. 1 (500 m offshore). Subplot A shows the modeled cross-shore velocity, B shows the measured cross-shore velocity. Subplot C and D show the alongshore modeled and measured velocity respectively. Positive velocities are towards the North (A,B) and East (C,D). The ADCP measures up to the instantaneous water level. This water level varies between the troughs and crests in the presence of the waves. As the ADCP bins are fixed this means that the upper bin only measures during the passing of the crests of the waves leading to a bias in the in the average flow velocity in the direction of wave propagation. For this reason the upper bins are not shown.

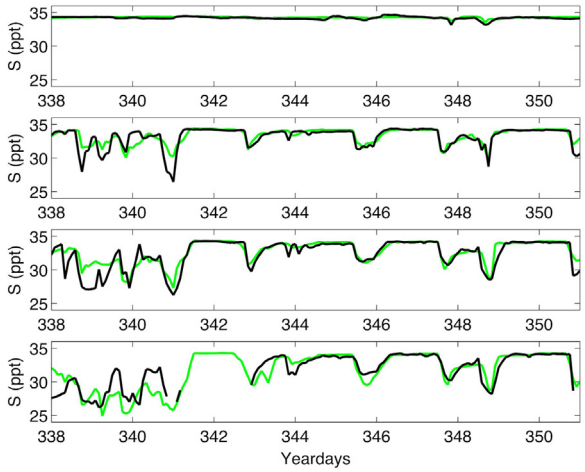

Fig. 3. Verification of the time dependent salinity 25 cm above the bottom at four different positions in the cross-shore array at A in Fig. 1. The black line denotes the measurements whereas the green line refers to the D3D simulation.

Table 1
Error quantification of D3D model. The positions of the stations are shown in the inset in Fig. 1.

Station	Quantity	RMSE (PPT - m/s)	Bias (PPT - m/s)	R^2
1	Salinity (PPT)	0.19	0.07	0.56
	Velocity (m/s)	0.09	−0.01	0.61
3	Salinity (PPT)	0.91	0.17	0.73
	Velocity (m/s)	0.07	−0.01	0.60
5	Salinity (PPT)	1.12	0.34	0.78
	Velocity (m/s)	0.07	−0.01	0.43
6	Salinity (PPT)	1.44	−0.15	0.74

$$RMSE = \sqrt{\overline{(p_i - o_i)^2}}, \tag{1}$$

$$Bias = \overline{(p_i - o_i)}, \tag{2}$$

$$R^2 = 1 - \frac{\overline{(p_i - o_i)^2}}{\overline{(o_i - \bar{o})^2} + \overline{(p_i - o_i)^2}}, \tag{3}$$

where p_i and o_i are the modeled and observed dataseries respectively. The model generally underestimates the velocities, however it reproduces the timing and depth of the plumes on e.g. YD 343, 347 and 348. This can be seen in the alongshore velocity signal - the blue spikes from the top downwards in subplots C and D in Fig. 2. This is important since the reliability of the simulation of coastal protection is based on these plumes. Moreover, full depth flow reversals, related to CAOs as discussed by Roth (2016), are also reproduced (e.g. YD 345) albeit weaker. This underestimation is related to the large scale model from which the boundary conditions are derived (HYCOM, 2013) during model verification. Cross-shore velocities are much weaker with the model showing similar time and spatial scales (Fig. 2). With respect to salinity, the model and the measurements compare well considering both the intrusion depth of the fresher plume as well as the timing for the period after YD 341. This is because before that period there were varying winds and many plumes overlapped. At the most offshore location (station 1 at 10 m depth), the effect of the plume is almost negligible in comparison to the effect at the other two stations 3. This relates to the fact that at this location the plume is detached from the bottom, which is also observed in the model. These comparisons show that the model is capable of hindcasting both the plume and the flow reversals under the observed river outflow, tides and wind forcing including COAs during SCOPE.

3.2. Lagrangian advection

To compute the LCS passive tracers are advected offline in the time and space dependent surface velocity fields that have been predicted by D3D. The paths of these tracers, which can be considered a proxy for oil pathways, can be calculated as,

$$\frac{\partial \vec{x}}{\partial t} = \vec{u}_{D3D}(\vec{x}, t) + \vec{u}_w(t)P, \tag{4}$$

where $\vec{x}$ is the horizontal space vector, t is time and $\vec{u}_{D3D}(\vec{x}, t)$ is the time and space dependent surface flow velocity. $\vec{u}_w(t)$ is the time dependent wind speed, which is taken constant in space. The windage factor is denoted with P, such that $\vec{u}_w(t)P$ is the velocity a tracer has due to the wind only and to which we refer as windage. This approach allows for varying the amount of windage, the number of tracers and the starting time of tracers simulations without having to rerun the Delft3D model. However, including the effects of varying tidal range, wind or river discharge requires rerunning Delft3D. Eq. (4) is solved with a fourth order Runge-Kutta method (Kutta, 1901). The maximum timestep for reliable calculations can be obtained by considering the Courant-Friedrich-Lewy (CFL) condition, based on Courant et al. (1928), and reads

$$C_{CFL} = \frac{u\Delta t}{\Delta x} + \frac{v\Delta t}{\Delta y} < 1, \tag{5}$$

where C_{CFL} is the CFL condition, u, v are flow velocities orthogonal to the grid at position x, y and Δt is the timestep. For the smallest grid cells and the highest velocities, one finds the following typical values, $x \geq 30$ m, $y \geq 60$ m, $u \leq 1$ m/s, $v \leq 1$ m/s. If a time step of $\Delta t = 20$ *sec* is taken, one obtains $C_{CFL} = 1$, which should give reliable results. Note that for the greatest portion of the grid, grid cells are much larger and most of the time, velocities much lower, leading to far lower values for C_{CFL}. In the yellow edged domain in Fig. 1, 30,000 (300 in the zonal and 100 in the meridional direction) tracers are released.

3.3. Lagrangian coherent structures

LCS are determined in order to visualize zones of high convergence and/or shearing such as those arising from the plume or the coastal current. In order to find LCS, the Finite Time Lyapunov Exponent (FTLE) field is calculated based on the pathways of the advected tracers discussed in Section 3.2. The FTLE measures the rate of separation of a group of tracers where the maximum is taken over all spatial orientations of the pair (Schindler et al., 2012). A group of tracers consists of five tracers, with one in the center, one on each side in the zonal direction and one on each side in the meridional direction. Mathematically the FTLE, σ can be found as,

$$\sigma(\vec{x}, t_0, t) = \frac{1}{t - t_0} \ln \sqrt{\lambda_{max}(\vec{C})}, \tag{6}$$

where t, t_0 are the time after and before advection respectively. $\lambda_{max}(\vec{C})$ denotes the largest eigenvalue of the right Cauchy Green deformation tensor $\vec{C}$.

Instead of separation, it is the aim to find convergence or shearing. If one advects tracers in backwards time, hence calculating where they come from, one finds that positions of greatest attraction/shearing coincide with high FTLE values. For this reason ridges of high FTLE values in the FTLE field reveal zones of atraction/shearing (Shadden, 2006; Haller, 2011).

The quality of the FTLE ridge in terms of visualization (sharpness and height) is determined by the advection time of tracers. The longer the backward advection time, the greater the separation of tracers that originate at a line of convergence and hence the greater $\lambda_{max}(\vec{C})$. Since different processes are dominant over different timescales, the advection time determines what processes are visible in the FTLE field. The

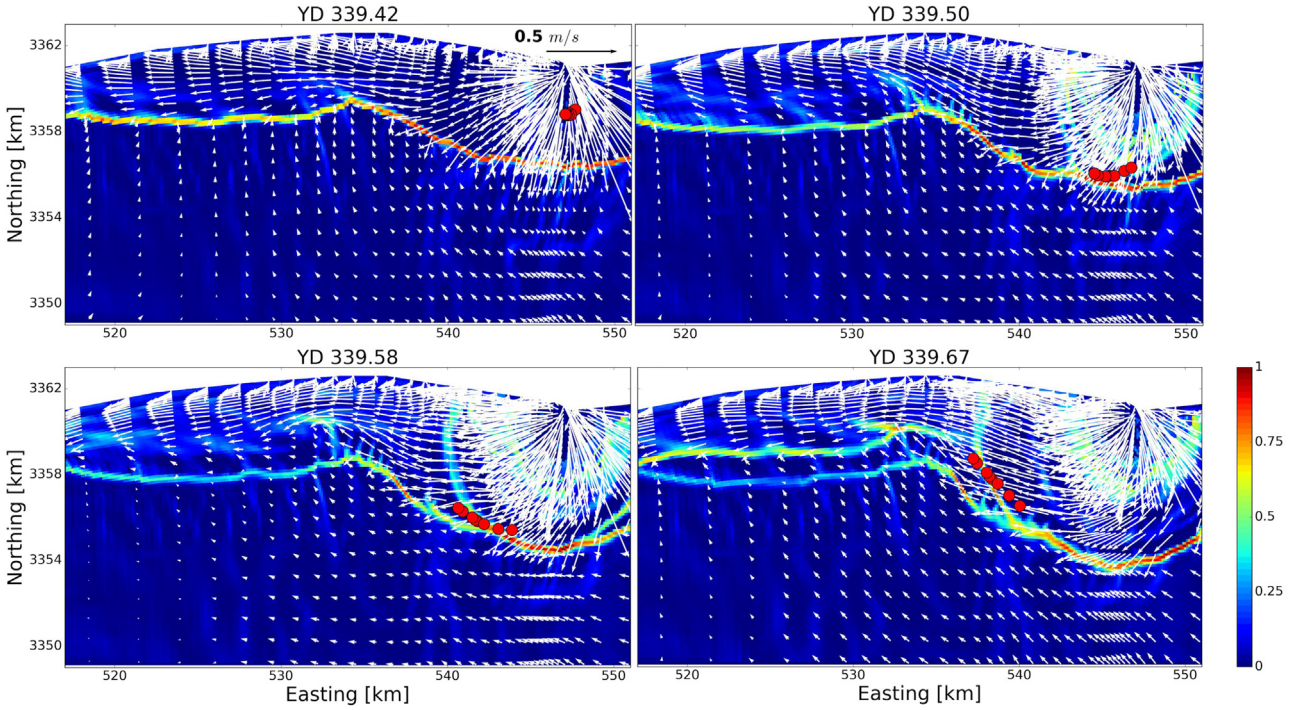

Fig. 4. Timeseries of FTLE fields, the higher the FTLE value, the more convergence and/or shearing. The colorbar denotes the normalized FTLE values. The white arrows visualize modeled surface flow fields. Real drifters deployed during SCOPE (denoted by the red dots) on YD 339 are plotted on top. (For interpretation of the references to color in this figure legend, the reader is referred to the web version of this article.).

timescale of the plume is related to the tide, which has a period of approximately one day. Longer advection times would thus show the effect of more than a single tidal cycle which is undesirable and limits the advection time to a maximum of one day. On the other hand, if one considers the shortest advection time possible, one should note that tracers must be allowed sufficient time to propagate at least the width of the plume front, which is approximately O(100 m) for the Choctawhatchee river plume (Huguenard et al., 2016). This leads to an advection time of at least several minutes. Within this range (5 min - 24 h) tests were carried out and those with an advection time of 2 h resulted in clear ridges at the location of the plume front while still minimizing the total calculation cost. Besides that, there were no other processes with this timescale, which excludes the chance on false positives. In total twelve sets of tracers were advected. Each subsequent set was released when the former set was advected for two hours. In total 24 h were covered, leading to twelve assessments of plume structure per tidal cycle.

In order to verify the location and development of the plume as a transport barrier, the FTLE fields of the plume are compared with the positions of real drifters deployed during SCOPE in Fig. 4. The drifters are deployed in the ebbing plume and rapidly move offshore to the edge of the plume as expected in the near-field plume with $Fr > 1$. There they stall and start moving in the alongshore direction parallel to the FTLE ridge, which supports the notion that the plume front can act as a surface transport barrier. The modeled velocity fields show the effect of both convergence and shearing on the FTLE values. In the snapshot of YD 339.42, convergence can be noted at the edge of the plume (3357 km Northing, 545 km Easting) as the surface velocity moving in opposite directions. Shearing (and some convergence) can be observed at the edge of the coastal current (3358.5 km Northing, 525 km Easting).

3.4. Time averaged Lagrangian coherent structures

The LCS described in Section 3.3 are snapshots of the position of the plume and the coastal current. Their position and accordingly their capability to protect the shore varies with time. Since oil might come from the entire Southern half of the windrose and at any time, it is needed to take the time-averaged protection due to the plume into account. The actual calculation of this protection is described in Section 3.5. In order to get an idea of the location and extent of the plume in thime, the FTLE field is averaged in time at each point in the field over five days after one day of spin up time. At positions where the plume or another flow feature stagnates, high values and more protection are expected. At positions where there is never a plume or the plume moves through rapidly, low averaged FTLE values are expected.

3.5. Tracer advection to determine beaching

In the previous section it has been discussed how to visualize the location and the extent of the plume and the coastal current. In order to verify whether these structures are effective in preventing oil from washing ashore, advection of oil is simulated by tracer advection for 24 h (a full tidal cycle) so tracers that originate far offshore O(20 km) are allowed the time to reach the shore. In order to reduce the influence of the tidal phase at the time of release of the tracers, a new set is advected every 4 h. This is done for all forcing conditions and windage parameters P. A tracer beaches when it arrives at a predefined beach grid cell, and the corresponding time and position of beaching are saved.

Time averaged statistics on where tracers beach and where those that beach originate from can now be compared to the time averaged FTLE fields, based on which the effectiveness of the plume as protection mechanism can be determined.

3.6. Forcing simulations

Wind forcing was simulated for two wind speeds, 3 and 6 m/s towards 8 directions (N, NW, W, SW, S, SE, E, NE). As discussed in Section 2, cross-shore winds related to CAOs drive alongshore flows. In the appendix, a derivation is given on how these alongshore flows are modeled. In order to understand the effect of windage on the oil fate,

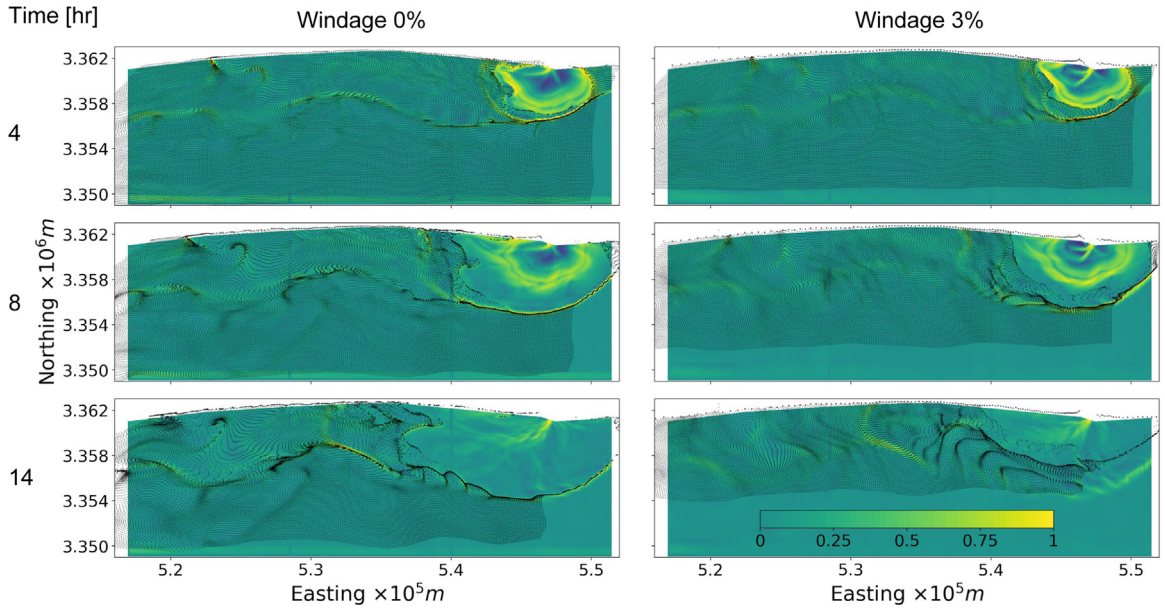

Fig. 5. A sequence of snapshots of tracers, the black dots (4, 8, 14 hrs integration time resp.) over FTLE fields (2 hrs integration time). The warmer colors denote zones of high FTLE values, hence convergence or shearing which coincides with the plume front. Note that the semi-circular bulge near the inlet is partly hidden by the high number of tracers plotted on top of them. Left column, simulation without windage. Right column simulation with 3% windage in advected tracers and FTLE field for three different timesteps. Tracers are released after more than a day of spin-up time. Wind to North, 3 m/s, tidal range 0.6 m, river discharge 188 m^3/s.

two values for the windage parameter were taken, $P \in 0, 3\%$. The effect of the tide was examined by taking the following two values, $A \in 0.3, 0.6\ m$. The influence of the river discharge was assessed by using $D \in 188, 500\ m^3/s$ respectively. This results in a total number of 128 computations for the forcing conditions considered.

4. Results

4.1. River plume as a time and space dependent transport barrier

If the plume fronts are true transport barriers (forward time) tracers are expected to line up with these fronts (ridges in the FTLE field) and follow the fronts in time. This is visualized in Fig. 5 by showing the FTLE field and the positions of advected tracers for three subsequent points in time. Since windage is an important parameter for the fate of oil, the snapshots are shown with and without the effect of windage. During the initial phase - 4 and 8 h after the tracers were released - the tracers line up with the near-field front, East of $5.4 \times 10^5\ m$. This happens for both cases, with and without windage. After 14 h the position of the plume front has propagated further South and the strength of the front has weakened (the color of the LCS is less warm) for both cases, with and without windage. In case of no windage, the LCS front and the tracers still align. However in the case of windage, these do not line up anymore and the plume does thus not act as a perfect flow barrier. As discussed, the plume position is visualized by making use of 2 h time integration, which means that over the last two hours the greatest convergence/shearing has occurred in the yellow/red zones, i.e. the plume front. On the other hand, the positions of the tracers are the integrated effect of 14 h of forward advection. These tracers were lined up at the near-field front during the initial part of the falling tide when the front was still strong. At a later stage, the front is still existent though much weaker and the wind pushes the tracers through the front. This explains why a semi-circular pattern in the positions of the tracers is still observed and why this pattern does not align with the position of the front. It thus shows that the persistence of the front as a surface transport barrier is limited to the zone near the inlet and only for a certain part of the tidal cycle.

Continuing in time, the tracers are pushed towards the shore by the wind and deflected by the ambient current. This leads to beaching of tracers, however the river plume causes a significant redistribution of where the tracers arrive at the shore. Furthermore, at a certain point in time the tide is rising again and tracers may be attracted by the inlet.

It can therefore be concluded that coastal protection due to the plume front is time and space dependent. In order to contemplate the effects of an oil spill throughout a full tidal cycle, an understanding of the the time averaged protection is needed and has to be verified with time averaged data on where tracers wash ashore.

4.2. Time averaged coastal protection

This paragraph describes the chance of tracers to beach, where they beach and from where they originate. Time averaged FTLE fields are obtained by averaging the FTLE value at each point in the grid for all time instants after the spin-up time. In order to calculate the chance a tracer beaches originating from a certain location, the following is done. For each block of 10×10 tracers around the dots in Fig. 6 the total number of tracers that reach the shore for all deployed sets - 5 days, 6 sets for 24 h advection - is calculated. This number is divided by the total number of advected tracers around that origin location to give the chance of beaching for that origin location. The total number of arriving tracers throughout the simulation after spin-up normalized by the length of the stretch as span up by a predefined beaching grid cell is calculated as to determine the chance of beaching at each beach location. The results are shown in Fig. 6.

The area of the plume is clearly visible as the semi-circular shape South of the inlet. Close to the inlet, high FTLE values can be observed which relate to the strong convergence of the plume when it just comes out of the inlet. The lighter yellow outer extent of the semi-circular plume has much lower convergence but shows up since the plume tends to slow down at this offshore extent which leads to relatively high FTLE values in a time averaged sense. The edge of the coastal current - the shore parallel yellow zone - features high flow shearing, hence not necessarily a barrier. Since the location of the edge of the coastal current is relatively stable, high FTLE values in a time averaged sense are obtained. It can be observed that the time averaged FTLE fields are only influenced by windage to a minor extent, which relates to the fact that

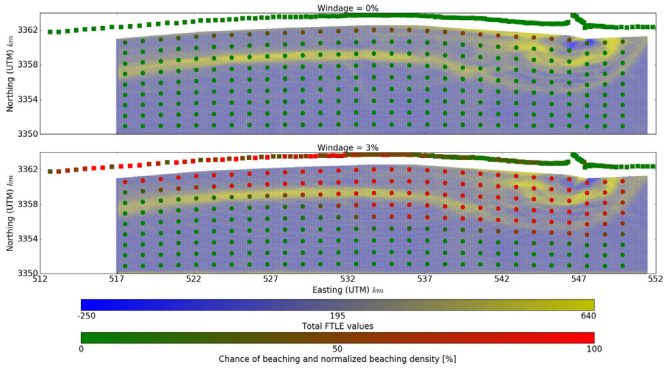

Fig. 6. Time averaged FTLE fields, overlaid with the average chance of beaching for tracers originating around a dot in FTLE field and the normalized number of beaching tracers along the beach shown at the gridpoints of the D3D model. The upper colorbar denotes the FTLE values, where the more positive values denote convergence and shearing (the plume front and the edge of the coastal current). The lower colorbar denotes the average chance of beaching at an origin location for the dots. The same colorbar is used for the beaching density (number of beaching tracers at a beach location normalized by stretch length). In the top plot there is no windage, whereas there is 3% windage in the lower plot. For both plots, wind to NW, 3 m/s, tidal range 0.3 m, river discharge 500 m^3/s.

the flow features are not fundamentally altered due to the windage. The effect of windage from other wind directions will be discussed in Section 4.3.

On the other hand, the number of tracers that beach is increased greatly in case windage is included. This can be seen from the colors of the dots, relating to the number of tracers that beach for each origin position. It can also be seen from the colors at the beach. Especially West from the near field, an increase in the number of beaching tracers is observed. The location of this increase is related to the Westernmost extent of the plume front, where the coast becomes relatively unprotected. Windage allows tracers from farther offshore to beach, which means that these tracers cross the plume and coastal current structures. However, one should note that the amount of beaching tracers originating from outside the plume and coastal current structures is much lower than the amount from inside these structures.

The plume and coastal current are not able to completely prevent oil from washing ashore, however their strongest influence lies in redistributing where oil washes ashore. This can be seen from the colored squares at the location of the beach. When comparing the plot with and without windage, one first observes that there is much more beaching when windage is included. Besides that, it can be noted that close to (and inside) the inlet, the number of beaching tracers is low, whereas this number starts to increase at approximately the maximum extent of the yellow semi circular bulge (537 km Easting). For the near field, where the Froude number is $Fr > 1$ and one observes the the semi

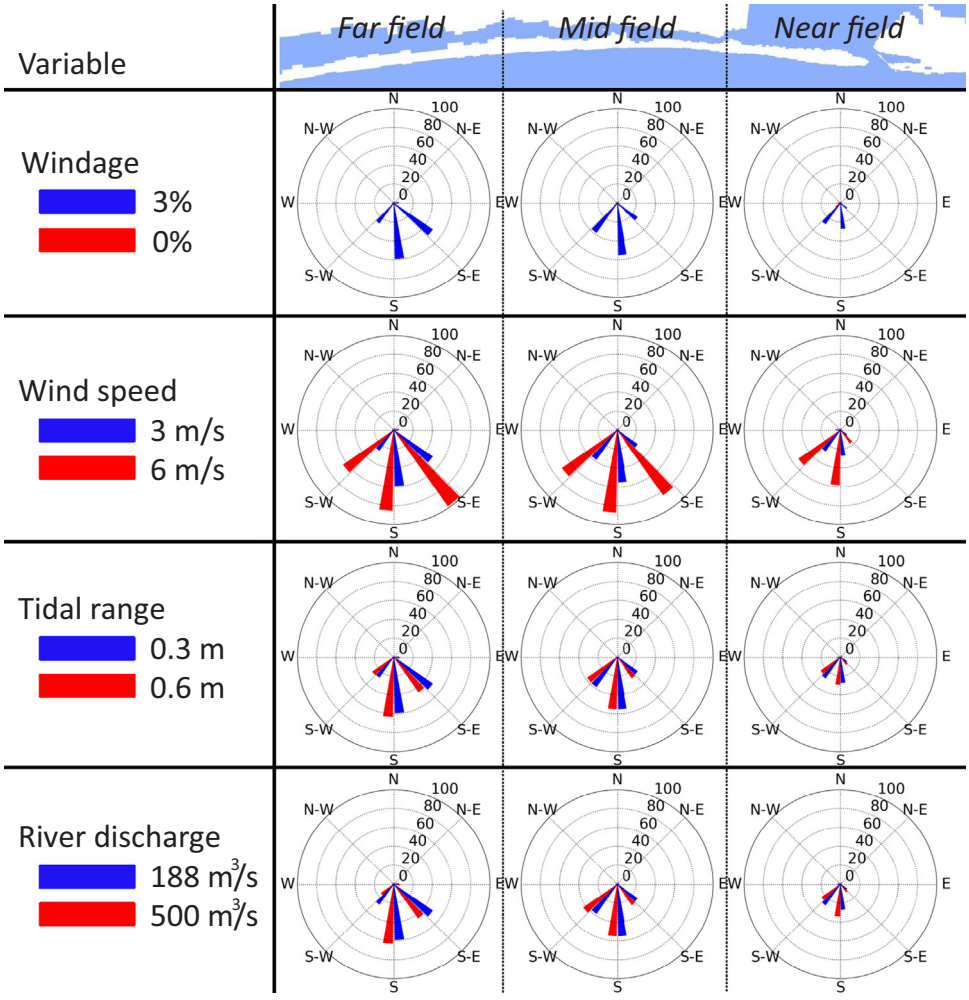

Fig. 7. Overview of the effect of different forcing types on the amount of beaching tracers. The number of beaching tracers compared to the number of released tracers is given as a percentage in the windroses and is shown for three coastal stretches and for a variation in four forcing types. Each windrose consists of two bars (different forcing) centered in a direction relating to where the wind comes from. The wind direction is the same for both bars (forcings). Note that for the lower three rows windage is taken at 3%.

circular bulge, one thus expects that the plume is effective in reducing the amount of oil that beaches. This complies with the observations from Fig. 5, where the plume acts as a transport barrier near the inlet even under the influence of windage until the plume front has weakened too much. As mentioned earlier, the contribution of windage to the floating oil under 3 m/s winds is approximately 0.1 m/s, which is smaller than the flow velocity near the inlet during the phase the plume comes out of up to 0.3 m/s (see Fig. 2). As a result, oil is first pushed offshore. When the plume has weakened, oil continues to flow forced by winds and ambient currents. These winds redirect the oil onshore but as the ambient current pushes the oil alongshore, the actual beaching does only to a lesser extent occur near the inlet.

Considering the protective effect of the coastal current, note that beaching is relatively high and extended to the West. The coastal current is hence a poor protection mechanism, which is in accordance with the fact that the velocity in the coastal current has a very limited cross-shore component (as can for example be observed from Fig. 4), not allowing for any protection when there is onshore wind forcing.

4.3. Statistics on coastal protection for various forcing mechanisms

Up to this point, timeseries and averages are discussed for specific forcing sets - wind, tidal range and river discharge. An overview of the effects of these different forcings is given by calculating the percentage of beaching tracers from the total number of deployed tracers for the three fields as discussed in Section 2, far-, mid- and near field. This is done in a time averaged sense, that is, all beaching during all simulations after spin-up is taken into account. In order to show the effect of each type of forcing, a basic set of forcings is taken and one forcing type is adjusted for each row in Fig. 7. This basic set consists of wind from all eight directions, wind speed 3 m/s, tidal range 0.3 m and river discharge, 188 m^3/s.

The most important observation is that beaching occurs in case there is a windage effect on oil. Next, the wind direction is the major factor of influence for beaching. In general, offshore winds prevent beaching, whereas onshore winds lead to beaching. As mentioned, winds from the North (related to CAO's) and winds from the South lead to alongshore currents to the East and West respectively. Even though these alongshore currents affect the extend of the plume in the alongshore direction, the effect of these ambient currents on average beaching is negligible in comparison to the effect of the wind itself. However, the ambient currents do affect the position of beaching, which is of importance in case there are scattered oil slicks.

If one considers the differences between the fields, one observes that especially in the near field, there is much less beaching, which is in accordance with the observation in Section 4.2 that the plume is not capable of completely preventing oil from washing ashore in the near field, however it is effective in redistributing the oil to other stretches of the coast. It should be noted that the lower amounts of beaching in the far field under winds from the Southwest and in the near field under winds from the Southeast can partly be explained by the fact that a great share of the tracers that should beach in these fields under the mentioned winds, originates from outside the computational domain and are thus not taken into account.

The effect of the wind speed is very clear, when winds are onshore, stronger winds lead to more beaching. Again note that the plume is capable of reducing the amount of oil washing ashore in the near field, even for stronger winds, although the effect is less pronounced in that situation. This is due to the fact that stronger winds lead to more mixing of the plume and ambient water and therefore reduce its protective capabilities. Under 6 m/s winds from the North, the maximum offshore extent of the plume is half its value compared to under 3 m/s winds. As the plume remains semi-circular, a smaller stretch to both the East and the West from the inlet is protected and the protection lasts shorter.

The effect of both the tidal range and the river discharge on the amount of beaching oil is very small in the far- and mid field. This is due to the fact that the front of the plume does not reach these fields. The coastal current is located in these zones, however, no protection is expected due to this current under onshore winds. In the near field note that, under winds to the North, more beaching occurs for both a higher tidal range and a higher river discharge. This can be explained by the fact that an increase in both type of forcings leads to a stronger plume. Winds to the North lead to an ambient current to the West. The stronger plumes are capable of pushing oil against the ambient current - towards the East and outside the near field. When the front weakens, the ambient current redirects the oil to the West back into the near field, where it beaches due to the onshore winds. Weaker forcing is to a lesser extent capable of pushing the oil against the ambient currents, explaining the larger amount of beaching for stronger tidal and river discharge forcing under winds to the North. The opposite is true for winds to the Northeast. In this situation, the plume itself is pushed to the Northeast and the stronger the plume, the more oil it pushes to the East outside of the near field.

5. Discussion

In accordance with results found by Xia et al. (2011), who numerically investigated a very similar estuary system in the NGoMex, the plume was found to be most influenced by wind. Research by Roth et al. (2017) has shown that surface drifters (1% windage) bounce off the Choctawhatchee river plume under light onshore winds (<2 m/s) and hence do not beach when released outside the plume. This is in accordance with the limited beaching under light (3 m/s) onshore wind and no windage. On the other hand, it was found that when windage is taken into account or when winds are stronger, beaching occurs. The latter conditions occurred when oil from the DWH oil spill was present off the Florida Panhandle which led to the arrival of tar balls on the beach (Roth et al., 2017).

For this research only weak forcing - weak winds ($\vec{u}_w < 6\ m/s$) and no waves - is taken into account. However there are occurrences of stronger forcing, e.g. during hurricanes leading to strong winds and big waves. The most dominant effect of such forcing would be rapid mixing of the plume and ambient water thereby reducing the extent of the plume.

Besides that, it is of interest to include the effect of strong winds and waves and make use of a Eulerian Lagrangian approach that can track oil in a 3D sense, which is needed for the increased vertical mixing. This model could also include natural dispersion of oil due to wave action or sea turbulence (Fingas, 2014) for different types of oil, looking at surface tension, density and viscosity. It could even take natural effects such as weathering, evaporation, oxidation, biodegradation, and emulsification into account (EPA, 1999).

Outside the surfzone Stokes drift transports surface material onshore (Lentz and Fewings, 2012), which, if strong enough, might lead to oil crossing the flow convergence barrier at the edge of the plume, reducing coastal protection. The effect of wave breaking and consequent rip currents occurs mainly in the surfzone, which is a zone where the plume edge only resides shortly, limiting the effect on the protective plume edge. Inside the surfzone (independent of the plume), Very Low Frequency motions (VLF) form an important transport mechanism for floating material. These VLFs are related to pulsating rip currents and eddies originating from wave forcing. It is expected that, as these VLFs cause a streaky distribution of surface flotsam (Reniers et al., 2010), they will influence the location and concentration of beaching of oil. This type of results could be helpful for first responders.

Flow reversals tied to CAOs are of major importance for the flow in the innershelf of the NGoMex and hence for oil fate. These reversals are reproduced by the model although to a weaker extent. This might lead to lower protection of the coast due to the plume in the zone West of the inlet, since the plume would be pushed further East by the true (stronger) alongshore flows. A more thorough investigation on CAO's affecting the alonshore flow with the aim of finding an expression for

the alongshore ambient flow as a function of cross-shore wind and possibly other parameters could yield a more precise way of incorporating the effect of CAOs and hence enhance the prediction of where what oil patches wash ashore.

Predicting where oil washes ashore can be done in real time with the current numerical setup as the calculation speed of both the Eulerian and the Lagrangian schemes are much faster than real time. However a coupling with a larger scale model is needed that allows for tracers to enter the domain when predictions on oil washing ashore are to be made longer than 24 h in the future. This is because for these time scales the distance traveled of tracers becomes on the order of the numerical domain.

6. Conclusion

In this research coastal protection by a small scale river plume against an oil spill was investigated for the Choctawhatchee river plume in the NGoMex. The protective mechanism is based on surface material transport barriers at fronts of such plumes. It was found that wind forcing - both speed and direction - is the dominant parameter for the amount and location of oil washing ashore, as the wind directly influences oil fate through windage and determines the evolution of the river plume.

The direct effect of wind direction on oil washing ashore is trivial, offshore winds direct oil offshore, whereas onshore winds drive oil towards the coast. The effect of wind on the plume is threefold. First there is a large scale effect related to cold air outbreaks (winds from the North), driving ambient alongshore currents to the East and limiting the Westward extend of the plume. On the other hand winds from the South lead to ambient currents to the West and further the Westward extent of the plume. However, it should be noted that although wind related ambient currents lead to a different positioning of the plume, the effect of windage - allowing oil to cross the edge of the plume - neutralizes the potential coastal protection due to the plume in the mid- and far field. Second, the wind affects the plume influencing the offshore extent of the semi-circular bulge and a possible development of an alongshore coastal current. This semi-circular bulge often features a strong front which acts as a transport barrier in the near field.

For weak $\vec{u_w} \sim 3\ m/s$ onshore winds, the front of the river plume acts as a transport barrier redirecting oil offshore during the ebbing tide in the near field. When the tide is rising and the convergence at the plume front has weakened, oil may wash ashore under the influence of onshore winds. As a result oil is redistributed by the plume during approximately half the tidal cycle, which leads to a reduction in oil washing ashore in the near field, but not to a complete prevention of oil reaching the coast. The oil which is redistributed by the plume is likely to wash ashore in other regions depending on the wind and the ambient current. In the mid- and far field, a coastal current may be present, depending on the wind direction, however this coastal current is not capable of preventing oil from washing ashore, it is only effective in redistributing the oil further to the West.

For stronger winds $\vec{u_w} > 6\ m/s$, there is less protection. Though near the inlet the amount of oil washing ashore is still smaller than away from the inlet although this effect is more pronounced for weaker winds. The effect of the tidal range and river discharge is minor in comparison to the effects of the wind.

First responders aiming to reduce the damage on the coast are advised to first regard the current winds. In the case the wind is offshore directed, beaching is unlikely. On the other hand, during onshore winds beaching is likely. When determining what patch of oil will be beaching at a location that should be protected, it is advised to first consider the ambient alongshore current. The ambient current will most likely be to the East when winds were from the West and North during the previous days, and to the West for winds from the East and South. Current local winds together with the ambient currents determine the direction of the oil patch. Lastly, if the inlet or the coast in the direct vicinity is of interest, it could be helpful to note that during the falling tide these zones are relatively well protected by the river plume for weak winds.

Acknowledgments

This research was made possible in part by a grant from The Gulf of Mexico Research Initiative, and in part by Universiteitsfonds Delft. Data are publicly available through the Gulf of Mexico Research Initiative Information & Data Cooperative (GRIIDC) at https://data.gulfresearchinitiative.org (doi: [http://dx.doi.org/10.7266/N72F7KC4, http://dx.doi.org/10.7266/N7ST7MRS, http://dx.doi.org/10.7266/N7542KJ9]).

Appendix A. Derivation of cross-shore wind related ambient currents

Roth (2016) has shown that alongshore ambient currents in the NGoMex are related to CAOs. These alongshore currents are not reproduced by D3D as the domain is too small. However, these currents can be imposed to the model through the boundary conditions. Neumann boundary conditions are used, hence a waterlevel gradient must be known for the Eastern and Western boundary of the domain. These waterlevel gradients should only be a function the cross-shore winds (CAOs) - the tide was found to have a negligible effect on alongshore currents.

For the derivation, the starting point is the depth-averaged linearized alongshore momentum balance as given by Lentz and Fewings (2012),

$$\frac{\partial V}{\partial t} + f(U + U_{st}) = -\frac{1}{\rho_0 h}\int_{-h}^{0}\frac{\partial P}{\partial y}dz + \frac{\tau^{sy} - \tau^{by}}{\rho_0 h} - \frac{1}{\rho_0 h}\left(\frac{\partial S^{xy}}{\partial x} + \frac{\partial S^{yy}}{\partial y}\right) - \frac{\tau^{bwy}}{\rho_0 h}, \tag{A.1}$$

where V is the depth-averaged alongshore velocity, f is the Coriolis frequency, U is the depth-averaged cross-shore velocity, U_{st} is the depth-averaged cross-shore velocity due to Stokes drift, ρ_0 is a reference water density, h is the water depth, P is the pressure and y is the alongshore direction. The vertical direction is denoted with z and τ^{sy}, τ^{by} refer to the surface and bottom stress respectively. The parameters S^{xy}, S^{yy}, τ^{bwy} refer to the radiation stresses and bottom stress due to surface gravity waves and x refers to the alongshore direction. When steady state is assumed and the effect of waves is neglected, the first (left hand side) and the last two terms (right hand side) can be neglected. Moreover, recall that only cross-shore winds are taken into account, this leads to zero alongshore wind stress, $\tau^{sy} = 0$. Lastly, the the Coriolis term is neglected, as U should be relatively small near the coast as it forms a natural cross-shore flow barrier. This leaves us with a pressure gradient and a bottom friction. It is assumed that the pressure gradient is purely barotropic. Near inlets this might not be the case, but the influence of the baroclinic pressure gradient is expected to be small compared to the influence of the barotropic pressure gradient on the scale of the entire Northeastern Gulf of Mexico. The latter assumption allows to approximate the alongshore pressure gradient as a waterlevel gradient,

$$\frac{\partial P}{\partial y} \approx \rho_0 g\frac{\partial \eta}{\partial y}, \tag{A.2}$$

Where η is the waterlevel. Integration to depth and realizing that the waterlevel gradient is not depth dependent leads to,

$$\frac{1}{\rho_0 h}\int_{-h}^{0}\frac{\partial P}{\partial y}dz = g\frac{\partial \eta}{\partial y}, \tag{A.3}$$

where h is the waterdepth. One can thus write Eq. (A.1) as,

$$g\frac{\partial \eta}{\partial y} = \frac{\tau^{by}}{\rho_0 h} \tag{A.4}$$

In order to express the bottom stress in terms of the flow velocity, various expressions as used in D3D are combined (Deltares, 2011) as,

$$\tau^{by} = \frac{\rho_0 g n^2 |V| V}{h^{1/3}}, \tag{A.5}$$

where $n = 0.028\frac{s}{m^{1/3}}$ is a Manning factor. One ADCP was left after the SCOPE experiment for long term measurements. Alongshore flow data from this ADCP was compared to wind data, from which it could be determined that $V \sim u_w/50$ - the cross-shore wind velocity u_w was roughly 50 times faster than the alongshore flow velocity.

Hence one finds,

$$\frac{\partial \eta}{\partial y} = \frac{n^2 \frac{u_w}{50}\left|\frac{u_w}{50}\right|}{h^{\frac{8}{6}}}. \tag{A.6}$$

It is anticipated that the waterlevel gradient should not be depth dependent. This relation is derived for a waterdepth of $h = 10\,m$, for the calculations this value is taken as fixed. For a given cross-shore wind speed, the alongshore waterlevel gradient can be calculated, which is needed for the neumann boundary conditions. This waterlevel gradient together with a value for the waterlevel halfway the offshore boundary can be used to calculate the waterlevel at each gridpoint along the offshore boundary, closing the system of equations.

References

Bianchi, T.S., Allison, M.A., Cai, W.-J., 2013. Biogeochemical Dynamics at Major River-Coastal Interfaces: Linkages with Global Change. Cambridge University Press.

Courant, R., Friedrichs, K., Lewy, H., 1928. Über die partiellen differenzengleichungen der mathematischen physik. Math. Ann. 100 (1), 32–74.

Deltares, 2011. User Manual Delft3D-FLOW.

EPA, USEPA., 1999. Understanding oil spills and oil spills response.

Fingas, M., 2014. A review of natural dispersion models. In International Oil Spill Conference Proceedings, 1, p. 285471, American Petroleum Institute.

Fiorentino, L., Olascoaga, M., Reniers, A., Feng, Z., Beron-Vera, F., MacMahan, J., 2012. Using lagrangian coherent structures to understand coastal water quality. Cont. Shelf Res. 47, 145–149.

Fong, D.A., Geyer, W.R., 2002. The alongshore transport of freshwater in a surface-trapped river plume. J. Phys. Oceanogr. 32 (3), 957–972.

Garvine, R.W., 1984. Radial spreading of buoyant, surface plumes in coastal waters. J. Geophys. Res.: Oceans 89 (C2), 1989–1996.

Garvine, R.W., 1987. Estuary plumes and fronts in shelf waters: a layer model. J. Phys. Oceanogr. 17 (11), 1877–1896.

Garvine, R.W., Monk, J.D., 1974. Frontal structure of a river plume. J. Geophys. Res. 79 (15), 2251–2259.

Gildor, H., Fredj, E., Steinbuck, J., Monismith, S., 2009. Evidence for submesoscale barriers to horizontal mixing in the ocean from current measurements and aerial photographs. J. Phys. Oceanogr. 39 (8), 1975–1983.

Graham, B., Reilly, W.K., Beinecke, F.G., Boesch, D., Garcia, T.D., Murray, C.A., Ulmer, F., 2011. The Use of Subsurface And Subsea Dispersants During The BP Deepwater Horizon Oil Spill. Draft. Tech. rep. National Commission on the BP Deepwater Horizon Oil Spill and Offshore Drilling.

Haller, G., 2011. A variational theory of hyperbolic lagrangian coherent structures. Phys. D: Nonlinear Phenom. 240 (7), 574–598.

Hetland, R.D., 2005. Relating river plume structure to vertical mixing. J. Phys. Oceanogr. 35 (9), 1667–1688.

Horner-Devine, A.R., Jay, D.A., Orton, P.M., Spahn, E.Y., 2009. A conceptual model of the strongly tidal columbia river plume. J. Mar. Syst. 78 (3), 460–475.

Horner-Devine, A.R., Hetland, R.D., MacDonald, D.G., 2015. Mixing and transport in coastal river plumes. Annu. Rev. Fluid Mech. 47, 569–594.

Hsueh, Y., Golubev, Y., 2002. A numerical model calculation of the flow in desoto canyon in response to northerly wind bursts in winter. Gulf Mex. Sci. 20 (1), 44–59.

Huguenard, K., Bogucki, D., Ortiz-Suslow, D., Laxague, N., MacMahan, J., Özgökmen, T., Haus, B., Reniers, A., Hargrove, J., Soloviev, A., et al., 2016. On the nature of the frontal zone of the choctawhatchee bay plume in the gulf of mexico. J. Geophys. Res.: Oceans 121 (2), 1322–1345.

Huh, O.K., Rouse, L.J., Walker, N.D., 1984. Cold air outbreaks over the northwest florida continental shelf: heat flux processes and hydrographic changes. J. Geophys. Res.: Oceans 89 (C1), 717–726.

Hurlburt, H.E., Thompson, J.D., 1982. The dynamics of the loop current and shed eddies in a numerical model of the gulf of mexico. Elsevier Oceanogr. Ser. 34, 243–297.

HYCOM (2013). Hycom + ncoda gulf of mexico 1/25° analysis (goml0.04expt_31.0), ⟨https://hycom.org/data/goml0pt04/expt-31pt0⟨, (Accessed 30 September 2015).

Kennish, M.J., 2000. Practical Handbook of Marine Science. CRC Press.

Kourafalou, V.H., Androulidakis, Y.S., 2013. Influence of mississippi river induced circulation on the deepwater horizon oil spill transport. J. Geophys. Res.: Oceans 118 (8), 3823–3842.

Kutta, W., 1901. Beitrag zur näherungweisen integration totaler differentialgleichungen. zeitschrift fur mathematik und und physik 46, 435–453.

Lentz, S.J., Fewings, M.R., 2012. The wind-and wave-driven inner-shelf circulation. Annu. Rev. Mar. Sci. 4, 317–343.

Lesser, G., Roelvink, J., Van Kester, J., Stelling, G., 2004. Development and validation of a three-dimensional morphological model. Coast. Eng. 51 (8), 883–915.

Marmorino, G., 1982. Wind-forced sea level variability along the west florida shelf (winter, 1978). J. Phys. Oceanogr. 12 (5), 389–405.

Mitchum, G.T., Clarke, A.J., 1986. Evaluation of frictional, wind-forced long-wave theory on the west florida shelf. J. Phys. Oceanogr. 16 (6), 1029–1037.

Morris Jr, J.G., Grattan, L.M., Mayer, B.M., Blackburn, J.K., 2013. Psychological responses and resilience of people and communities impacted by the deepwater horizon oil spill. Trans. Am. Clin. Climatol. Assoc. 124, 191–201.

Murphy, P.L., Waterhouse, A.F., Hesser, T.J., Penko, A.M., Valle-Levinson, A., 2009. Subtidal flow and its variability at the entrance to a subtropical lagoon. Cont. Shelf Res. 29 (20), 2318–2332.

NOAA (2017). National data buoy center, ⟨http://www.ndbc.noaa.gov/station_page.php?Station=42012⟩.

O'Donnell, J., Marmorino, G.O., Trump, C.L., 1998. Convergence and downwelling at a river plume front. J. Phys. Oceanogr. 28 (7), 1481–1495.

Olascoaga, M., Beron-Vera, F., Haller, G., Trinanes, J., Iskandarani, M., Coelho, E., Haus, B., Huntley, H., Jacobs, G., Kirwan, A., et al., 2013. Drifter motion in the gulf of mexico constrained by altimetric lagrangian coherent structures. Geophys. Res. Lett. 40 (23), 6171–6175.

Poje, A.C., Özgökmen, T.M., Lipphardt, B.L., Haus, B.K., Ryan, E.H., Haza, A.C., Jacobs, G.A., Reniers, A., Olascoaga, M.J., Novelli, G., et al., 2014. Submesoscale dispersion in the vicinity of the deepwater horizon spill. Proc. Natl. Acad. Sci. 111 (35) (12,693-12,698.).

Reed, M., Turner, C., Odulo, A., 1994. The role of wind and emulsification in modelling oil spill and surface drifter trajectories. Spill Sci. Technol. Bull. 1 (2), 143–157.

Reed, M., Johansen, Ø., Brandvik, P.J., Daling, P., Lewis, A., Fiocco, R., Mackay, D., Prentki, R., 1999. Oil spill modeling towards the close of the 20th century: overview of the state of the art. Spill Sci. Technol. Bull. 5 (1), 3–16.

Reniers, A.J., MacMahan, J., Beron-Vera, F., Olascoaga, M., 2010. Rip-current pulses tied to lagrangian coherent structures. Geophys. Res. Lett. 37, 5.

Roth, M., (2016). Material transport in the inner shelf of the northern gulf of mexico. Ph. D. Thesis, Naval Postgraduate School, Monterey, CA, unpublished thesis.

Roth, M.K., MacMahan, J., Reniers, A., Özgökmen, T.M., Woodall, K., Haus, B., 2017. Observations of inner shelf cross-shore surface material transport adjacent to a coastal inlet in the northern gulf of mexico. Cont. Shelf Res. 137, 142–153.

Schaeffer, B., 2010. Choctawhatchee bay. In: A presentation to the pensacola public workshop, february 10, 2010, in support of the development of numeric nutrient criteria in florida estuaries and coastal waters., ⟨http://www.dep.state.fl.us/water/wqssp/nutrients/estuarine.htm⟩.

Schindler, B., Peikert, R., Fuchs, R., Theisel, H., 2012. Ridge Concepts for the Visualization of Lagrangian Coherent Structures, in Topological Methods in Data Analysis and Visualization II. Springer, pp. 221–235.

Seim, H., Kjerfve, B., Sneed, J., 1987. Tides of mississippi sound and the adjacent continental shelf. Estuar., Coast. Shelf Sci. 25 (2), 143–156.

Shadden, S.C., (2006), A dynamical systems approach to unsteady systems. Ph.D. Thesis, California Institute of Technology.

Smith, L.C., Smith, M., Ashcroft, P., 2010. Analysis of environmental and economic damages from british petroleum's deepwater horizon oil spill. Albany Law Rev. 74 (1), 563–585.

Smith, S., Banke, E., 1975. Variation of the sea surface drag coefficient with wind speed. Q. J. R. Meteorol. Soc. 101 (429), 665–673.
Smithsonian, 2016. Smithsonian institution's ocean initiative: Gulf oil spill, ⟨http://ocean.si.edu/gulf-oil-spill⟩.
Upton, H.F., 2011. The deepwater horizon oil spill and the gulf of mexico fishing industry. Tech. rep., Congressional Research Service, Library of Congress.
USGS, 2016. Usgs 02365500 choctawhatchee river at caryville. fla., ⟨http://waterdata.usgs.gov/fl/nwis/uv?Site_no=02365500⟩.
Valle-Levinson, A., Huguenard, K., Ross, L., Branyon, J., MacMahan, J., Reniers, A., 2015. Tidal and nontidal exchange at a subtropical inlet: destin inlet, northwest florida. Estuar. Coast. Shelf Sci. 155, 137–147.
Velasco, G.G., Winant, C.D., 1996. Seasonal patterns of wind stress and wind stress curl over the gulf of mexico. J. Geophys. Res.: Oceans 101 (C8) (18,127-18,140).
Xia, M., Xie, L., Pietrafesa, L.J., Whitney, M.M., 2011. The ideal response of a gulf of mexico estuary plume to wind forcing: its connection with salt flux and a lagrangian view. J. Geophys. Res.: Oceans 116 (C8).